Tuning the optical bandgap in multi-cation compound transparent conducting-oxides: The examples of In_2ZnO_4 and $In_4Sn_3O_{12}$

Fernando P. Sabino, Luiz N. Oliveira, Su-Huai Wei, and Juarez L. F. Da Silva

---

Articles you may be interested in

A comprehensive study of g-factors, elastic, structural and electronic properties of III-V semiconductors using hybrid-density functional theory
Journal of Applied Physics **123**, 065702 (2018); 10.1063/1.5018325

Guest Editorial: The dawn of gallium oxide microelectronics
Applied Physics Letters **112**, 060401 (2018); 10.1063/1.5017845

Gallium diffusion in zinc oxide via the paired dopant-vacancy mechanism
Journal of Applied Physics **123**, 055701 (2018); 10.1063/1.5000123

Rethinking the theoretical description of photoluminescence in compound semiconductors
Journal of Applied Physics **123**, 055703 (2018); 10.1063/1.5008810

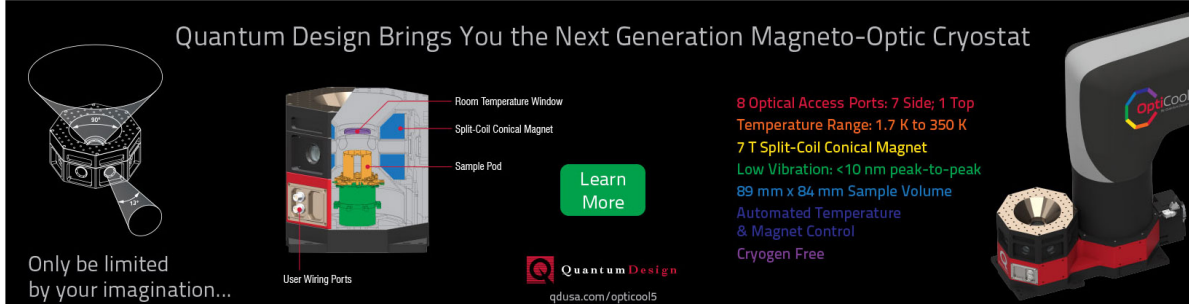Enhanced ultraviolet photo-response in Dy doped ZnO thin film
Journal of Applied Physics **123**, 054502 (2018); 10.1063/1.5015959

First-principles study of direct and indirect optical absorption in $BaSnO_3$
Applied Physics Letters **112**, 062106 (2018); 10.1063/1.5013641

Tuning the optical bandgap in multi-cation compound transparent conducting-oxides: The examples of In$_2$ZnO$_4$ and In$_4$Sn$_3$O$_{12}$

Fernando P. Sabino,[1,2,a)] Luiz N. Oliveira,[2,a)] Su-Huai Wei,[3,a)] and Juarez L. F. Da Silva[4,a)]

[1]*Department of Materials Science and Engineering, University of Delaware, Newark, Delaware 19716, USA*
[2]*São Carlos Institute of Physics, University of São Paulo, PO Box 369, 13560-970 São Carlos, SP, Brazil*
[3]*Beijing Computational Science Research Center, Beijing 100094, China*
[4]*São Carlos Institute of Chemistry, University of São Paulo, PO Box 780, 13560-970 São Carlos, SP, Brazil*

Transparent conducting oxides such as the bixbyite In$_2$O$_3$ and rutile SnO$_2$ systems have large disparities between the optical and fundamental bandgaps, ΔE_g^{OF}, because selection rules forbid dipolar transitions from the top of the valence band to the conduction-band minimum; however, the optical gaps of multi-cation compounds with the same chemical species often coincide with their fundamental gaps. To explain this conundrum, we have employed density-functional theory to compute the optical properties of multi-cation compounds, In$_2$ZnO$_4$ and In$_4$Sn$_3$O$_{12}$, in several crystal structures. We show that a recently proposed mechanism to explain the disparity between the optical and fundamental gaps of M$_2$O$_3$ (M = Al, Ga, and In) applies also to other binary systems and to multi-compounds. Namely, a gap disparity will arise if the following three conditions are satisfied: (*i*) the crystal structure has inversion symmetry; (*ii*) the conduction-band minimum is formed by the cation and O *s*-orbitals; and (*iii*) there is strong *p-d* coupling and weak *p-p* in the vicinity of the valence-band maximum. The third property depends critically on the cationic chemical species. In the structures with inversion symmetry, Zn (Sn) strengthens (weakens) the *p-d* coupling in In$_2$ZnO$_4$ (In$_4$Sn$_3$O$_{12}$), enhancing (reducing) the gap disparity. Furthermore, we have also identified a In$_4$Sn$_3$O$_{12}$ structure that is 31.80 meV per formula unit more stable than a recently proposed alternative model. *Published by AIP Publishing.* https://doi.org/10.1063/1.5018056

INTRODUCTION

Efficient transparent conducting oxides (TCO) combine high transparency in the visible spectrum with nearly metallic electrical conductivity. TCOs have been applied in a variety of devices, such as solar cells,[1] light emitting diodes,[2] and transparent transistors.[3–6] An outstanding example is tin-doped indium oxide (In$_2$O$_3$: Sn),[7] the prototypical TCO known as ITO. The relatively narrow fundamental bandgap and low conduction-band minimum of ITO favor *n*-type conduction.[8] One might expect the narrow band to likewise facilitate optical absorption in the visible spectrum. Yet, ITO is transparent, because a large number of forbidden optical transitions make the optical gap substantially larger than the fundamental band gap.

In the bixbyite In$_2$O$_3$ structure, for example, the disparity between the fundamental and optical bandgap, ΔE_g^{OF}, is of the order of 0.70 eV,[9,10] i.e., the fundamental gap is $E_g^F = 2.90$ eV, while the optical bandgap is $E_g^O = 3.60$ eV.[9] Unfortunately, In is expensive, and hence, much effort has been devoted to searching alternative TCOs with less In content, such as multi-cation compounds. Combinations of two or more oxides based on In$_2$O$_3$, Ga$_2$O$_3$, Al$_2$O$_3$, SnO$_2$, ZnO, or CdO have been studied as possible replacements for In$_2$O$_3$.[5,6,11–17]

Natural candidates are the combinations In$_2$O$_3$-SnO$_2$ (Ref. 11) and In$_2$O$_2$-ZnO,[13,18] which combines the outstanding properties of In$_2$O$_3$ and the smaller cost of Zn and Sn. In principle, we would have to transfer the properties of the binary oxides to the multi-cation oxides, but this may not be true. Consider, for example, InZn$_2$O$_4$ with its different crystal structures such as the spinel structure[19] and the monoclinic IZO model—a structure proposed by Da Silva *et al.*[13] that has been employed to study the 1In$_2$O$_3$-1ZnO composition. As demonstrated by the subsequent first-principles density-functional theory (DFT) computed by Walsh *et al.*,[18] the optical and fundamental bandgaps coincide for monoclinic IZO. The congruence between the optical and fundamental gaps indicates that while forbidden in bixbyite In$_2$O$_3$, the optical transitions between the valence band maximum (VBM) and the conduction band minimum (CBM) are allowed in monoclinic-IZO InZn$_2$O$_4$, and hence, it reduces the transparency of the multi-compound.

Another illustration is provided by the optical-absorption properties of In$_4$Sn$_3$O$_{12}$.[11] Measurements of the x-ray photoemission and optical absorption spectra point to a $\Delta E_g^{OF} \approx 0.60$ eV between the optical and fundamental band gaps,[17] a large disparity that has been traced to the allowed transitions, but weak, from states in the vicinity of VBM to the CBM. The spectrum of the multi-cation compound, therefore, contrasts with those of the binary oxides SnO$_2$ and In$_2$O$_3$, in which optical transitions from the VBM to the CBM are completely forbidden by dipole selection rules.[9,10,20–22]

a)Authors to whom correspondence should be addressed: fernandopsabino@yahoo.com.br; luizno@usp.br; suhuaiwei@csrc.ac.cn; and juarez_dasilva@iqsc.usp.br.

Sabino *et al.*[10] have proposed a mechanism that explains the gap disparity in the TCOs M_2O_3 (M = Al, Ga, and In) and opened the perspective of tuning the disparity in other oxides. Analyses of the band-structure data and optical-transition matrix elements resulting from DFT + U computations have identified three conditions controlling the emergence of a bandgap disparity:[10] (*i*) a crystal structure with an inversion symmetry; (*ii*) the CBM formed by the cation and O *s*-states; and (*iii*) a strong coupling between the cation *d*- and O *p*-states near the VBM.[10] Under the three conditions, the CBM and the states close to the VBM are even under inversion, which blocks dipolar transitions between these states.

This model and the absence of inversion symmetry in monoclinic-IZO In_2ZnO_4 (Ref. 18) explain the congruence between its optical and fundamental bandgaps. If the same argument were applied to the rhombohedral-ISO $In_4Sn_3O_{12}$ (Ref. 17) structure, however, we would conclude that the optical and fundamental bandgaps are identical, in disagreement with the experimental results.[17] The reasoning therefore seems to fail. Can the rule that describes binary TCOs be applied to the class of multi-cation compound TCOs? One would hope to have a positive answer, for then the model can be used to explain and predict new TCOs multi-cation compounds with optical band gap disparity.

With this goal in mind, we have computed optical spectra for the following multi-cation compounds: In_2ZnO_4 in the spinel and inverse-spinel (IS) crystal structures (the latter has low stability, and hence, it is an artificial structure); $In_4Sn_3O_{12}$ in the rhombohedral ISO structure;[17] and $In_4Sn_3O_{12}$ in a more stable crystal structure that we call ISO$_i$ (the Appendix contains a detailed discussion of this structure, which is 31.80 meV per formula unit more stable than rhombohedral ISO). Our results show that the disparity between the optical and fundamental bandgaps in the multi-cation TCOs follow the mechanism proposed in Ref. 10, i.e., the structural and electronic properties control the mismatch between the optical and fundamental gaps. Furthermore, we demonstrate that the composition based on In_2O_3-ZnO can generate a large disparity between the optical and fundamental bandgaps, a disparity that is not observed for In_2O_3-SnO_2. Our findings allow tuning of the optical bandgap in multi-cation TCOs.

THEORETICAL APPROACH AND COMPUTATIONAL DETAILS

Our periodic DFT[23,24] calculations were carried out within the semilocal Perdew–Burke–Ernzerhof (PBE) exchange-correlation functional.[25] The Kohn–Sham equation was solved using the all-electron projected augmented wave (PAW) method[26,27] as implemented in the Vienna *ab initio* simulation package (VASP), version 5.3.5.[28,29] Moreover, we have employed the PAW projectors provided within VASP, the following valence electrons being taken into account: O $2s^2 2p^4$, Zn $3d^{10} 4s^2$, In $4d^{10} 5s^2 5p^1$, and Sn $4d^{10} 5s^2 5p^2$.

To obtain the equilibrium crystal volumes, we have minimized the stress tensor and atomic forces on every atom, using a plane-wave cutoff energy of 600 eV and a $5 \times 5 \times 5$

k-point mesh in the Brillouin-zone integration for the spinel In_2ZnO_4 structure. The same **k**-point density was used for all the remaining systems. The electronic properties, such as the density of states, band structure, and optical properties, were computed using a cutoff energy of 450 eV and a higher **k**-point mesh.

Our computation of optical properties considered only direct transitions from the valence to the conduction band, while other excitations, such as indirect transitions and the ones involving excitonic states were excluded. To well define the optical-absorption threshold, we have applied a small Lorentzian broadening parameter of 5×10^{-4} eV to the dielectric constant, which is few orders of magnitude smaller than the value recommended by VASP, i.e., 0.1 eV. For that, we modified the linear_optic.F subroutine, which is now available within VASP for all users, and we thank G. Kresse for the support. The modification was necessary to increase the accuracy of the computed transition energies in the region close to the fundamental bandgap.

RESULTS

Crystal structures

As previously mentioned, our DFT calculation is performed for multi-cation compounds in the configuration 1(In_2O_3)-1(ZnO) and 2(In_2O_3)-3(SnO_2). For In_2ZnO_4, the literature reports stability studies of several structures. The spinel[19] and monoclinic IZO[13] are the most stable structures. The inverse-spinel In_2ZnO_4 structure has low stability due to the occupation of octahedral (tetrahedral) sites by Zn (In) atoms. Notwithstanding, we have included this structure in our computations to complement our understanding of the optical-property dependence on the crystal structure. In fact, for In_2ZnO_4, only the spinel and inverse-spinel structures had to be taken into account, since the results for monoclinic IZO have been reported by Walsh *et al.*[18] Two crystal structures were used to represent $In_4Sn_3O_{12}$. The first one is the structure reported by O'Neil *et al.*,[17] a rhombohedral phase that we call ISO. The second one is a modification of the ISO structure with the point symmetry of the experimental structure.[11] In contrast with ISO, the modified structure has an inversion symmetry, which is called ISO$_i$. We find that ISO$_i$ is more stable than ISO[17] by 31.80 meV per formula unit for $In_4Sn_3O_{12}$.

In brief, we have focused on four crystal structures, with two distinct chemical compositions. Further details on the crystal structures are described within the Appendix. The results provide insight into the disparity between optical and fundamental bandgaps in multi-cation TCOs and also predict good candidates, with respect to the optical properties, for other stoichiometric and cation compositions.

Band structure

Figure 1 depicts the band structures along two lines through the Γ-point for In_2ZnO_4 in the spinel and inverse spinel configurations and $In_4Sn_3O_{12}$ in the ISO, and ISO$_i$ configurations. The CBM lies at the Γ-point, while the energy difference between the second conduction band and
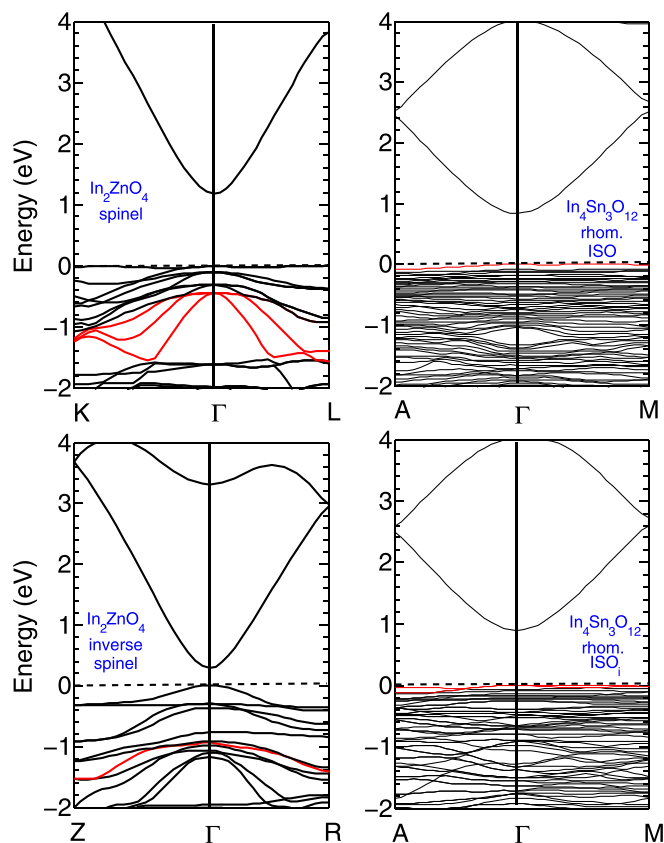
FIG. 1. Band structures for the multi-cation In_2ZnO_4 compounds based on the spinel and inverse-spinel structures, and for the $In_4Sn_3O_{12}$ compounds based on rhombohedral ISO and ISO_i models. The red bands identify the initial states for the allowed high-intensity transitions at the Γ-point. The dashed lines indicate the valence band maximum, from which energies are measured.

the CBM at Γ is larger than the fundamental bandgap. This condition reduces the probability of intra-band optical transitions and allows us to restrict our analysis to the Γ-point and its vicinity in the valence band and the CBM.

For In_2ZnO_4 in the spinel structure, the highest band is nearly flat, while the valence states below it show small dispersion around the Γ-point. This condition is very similar to the one found in bixbyite In_2O_3.[10,22] In the inverse-spinel structure, the highest occupied valence states are more delocalized, with the VBM at the Γ-point. For both multi-compounds, the bandgaps are direct, at the Γ-point.

The band structures of the $In_4Sn_3O_{12}$ system in the ISO and ISO_i model structures are very similar because the two configurations are only distinguished by the atomic positions of the Sn and In atoms, which yields an energy difference of few meV. However, due to the distinct symmetry between both ISO and ISO_i structures, some states are doubly degenerate in ISO_i, while only non-degenerate states occur in the ISO structure. Hence, the ISO structure exhibits more non-degenerate bands than the ISO_i structure.

It has been well documented that the underestimation of bandgaps by the PBE functional,[30–33] e.g., the PBE bandgap for $In_4Sn_3O_{12}$ in the rhombohedral ISO structure is 0.84 eV, while it increases slightly to 0.89 eV for the rhombohedral ISO_i structure, while the experimental value is 2.70 eV.[17] Assuming the same trend, we expect the PBE functional to

underestimate the fundamental gaps for spinel and inverse spinel In_2ZnO_4. Unfortunately, no experimental results are available to check the accuracy of the computed gaps, 1.18 eV and 0.29 eV for the spinel and inverse-spinel structures, respectively.

DENSITY OF STATES

Figure 2 depicts the local density of states for In_2ZnO_4 in the spinel and inverse-spinel structures and $In_4Sn_3O_{12}$ in the rhombohedral ISO and ISO_i models. In all the compounds, the O p-states are dominant in the valence band. In contrast, the conduction band mainly comprises O p-states and cation s-states, while the CBM is constituted only by the O and cation s-states. Previous work has shown that the positions of the cation d-states control several properties of the oxides. Examples are the relative stabilities of Ga_3O_2 crystal structures,[34] and the disparities between the optical and fundamental bandgaps in In_2O_3[9,10] and SnO_2.[22] The In d-state in bixbyite In_2O_3 lies deep in the valence band, while the Zn d-states in ZnO are spread in the valence band near the VBM. Due to the large number of electrons and electrostatic shielding, the Sn d-states in rutile SnO_2 lie deepest among the d-states in all the binary oxides used in our study of the multi-cation compounds. It follows that the coupling between the cation d-states and O p-states in the oxides grows in the following cation sequence: Sn, In, and Zn.

Similar results can be observed in the multi-cation compound phase, shown in Fig. 2. In the In_2ZnO_4 system, independently of crystal structure the cation d-states are heavily concentrated in two regions. The first region lies deep below the VBM, around –12 eV. Here, the d-states are associated with the In chemical species. The second region is broader and lies closer to the VBM, indicated by the color pink in Fig. 2, and it is associated with Zn atoms. We can conclude that in In_2ZnO_4 the cation d-states are strongly coupled to the O p-states.

Nevertheless, the crystal structure is responsible for the fine tuning of the p-d coupling. For example, closer to the VBM, the number of states with cation-d contribution is smaller for the spinel structure than for the inverse-spinel structure. The coupling is very important because it determines the parity of the wave functions near the VBM. Moreover, in the same region, the coupling between the cation p-states and the O p-states is smaller for the inverse-spinel structure. The larger the p-p coupling, the larger the number of even states close to the VBM.[22] Other structures, such as the monoclinic In_2ZnO_4 structure studied by Da Silva *et al.*[13] and Walsh *et al.*,[18] have densities of states similar to the spinel and inverse-spinel structures. Strong p-d coupling is a characteristic of the chemical composition in In_2ZnO_4.

By contrast, the p-d coupling in the $In_4Sn_3O_{12}$-based multi-cation compounds is weaker. In these materials, both the d-states of In and Sn are located deep inside the valence band, a situation similar to the bixbyite-In_2O_3 and rutile-SnO_2 binary oxides. Furthermore, the similarity between the crystal structures makes the couplings in the region very close to the vicinity of VBM nearly identical. This feature
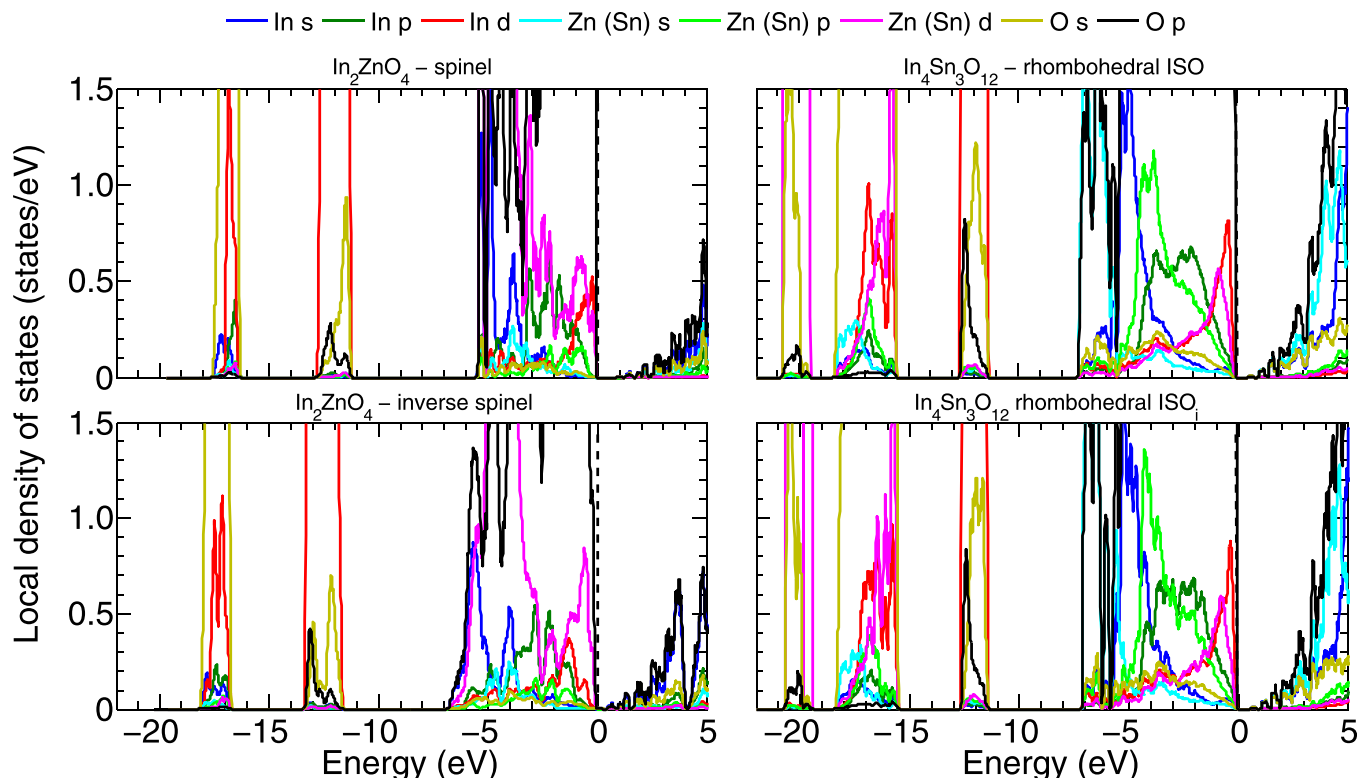
FIG. 2. Local density of states for In_2ZnO_4 in spinel, inverse-spinel, and for $In_4Sn_3O_{12}$ in rhombohedral ISO and ISO_i structures. The cations are numbered in order of occurrence in the chemical formula. The dashed lines indicate the valence band maximum, from which energies are measured.

makes the electronic properties of the two rhombohedral crystal structures very similar. In the system with inversion symmetry, the low *p-d* coupling favors odd parity for the electron wave functions with energies close to the VBM.[10] Under a broader perspective, we can see that the strength of the *p-d* (*p-p*) coupling depends on the cation composition of the TCO multi-cation compound. The couplings can, therefore, be controlled. More specifically, to strengthen (weaken) the *p-d* coupling in the vicinity of the VBM one should focus on In_2O_3-ZnO (In_2O_3-SnO_2) multi-cation compounds.

OPTICAL PROPERTIES

To gain a deeper understanding of the optical properties for In_2ZnO_4 in the spinel and inverse-spinel structures, and for $In_4Sn_3O_{12}$ in the rhombohedral ISO and ISO_i structures, we have computed the absorption coefficients and transition matrix elements and carried out symmetry analysis. To determine the irreducible representations of the computed bands, we have only examined the undistorted systems, i.e., the systems with relatively high symmetry, such as In_2ZnO_4 in the spinel structure and $In_4Sn_3O_{12}$ in the rhombohedral ISO_i model. In_2ZnO_4 in the inverse-spinel structure and $In_4Sn_3O_{12}$ in the rhombohedral ISO model are distorted. Their symmetry being, therefore, lower than that of the reference structure, symmetry analysis would be inconclusive.

Even for the low symmetry systems, the absorption-coefficient curves can be discussed on the basis of the computed amplitudes of the transition matrix elements. The absorption coefficients in the vicinity of the VBM are very

small, typically four orders of magnitude smaller than the coefficients in the following discussion. The corresponding transitions would only be detectable under very intense lighting. We have, therefore, computed the difference ΔE_g^{OF} between the optical and fundamental bandgaps at the Γ-point.

The disparity between the optical and the fundamental bandgap can be comparable to the experimental results despite the fact that fundamental bandgap is underestimated by the PBE exchange and correlation functional. There are two reason that support this argument: (1) The difference between the energies of occupied (unoccupied) states are slightly affected by the bandgap magnitude, in the region close to the VBM (CBM); (2) The symmetry obtained by the PBE functional are similar to the experimental results as shown by Sabino *et al.*[22] for SnO_2, for example. Based on these conceptions, Walsh *et al.*[9] used the PBE exchange and correlation functional to obtain $\Delta E_g^{OF} \approx 0.70$ eV, a value which is comparable to the experimental results.[9]

For all the studied TCOs, the CBM consists of cation and O *s*-states. It follows that the CBM remains invariant under all symmetry operations in the space group of each structure. The resultant irreducible representation are A_{1g} and A_g for spinel In_2ZnO_4 and rhombohedral ISO_i $In_4Sn_3O_{12}$, respectively – the only undistorted crystal structures. In_2ZnO_4 in the inverse-spinel structure has inversion symmetry, even though the non-uniform distribution of the cations in the unit cell (see the Appendix for the details of the crystal structure) introduces distortion. The electron wave functions in inverse-spinel In_2ZnO_4 can therefore be classified by parity.

The amplitudes of the transition matrix elements for spinel and inverse-spinel structured In_2ZnO_4 are shown in Table I. Also shown are initial- and final-state irreducible representations. Eigenstates are numbered in order of increasing energy taking the VBM as reference (0 eV energy). In the spinel (inverse-spinel) structure, transitions from the valence-band states 55–62 (57–62) to the conduction band number 63 are forbidden, and an optical to fundamental bandgap disparity of 0.44 eV (0.93 eV) arises.

To explain the striking difference between the two gap disparities, we have to compare the occupations of different cation sites in the two crystal structures. Especially important is the atom at the centrosymmetric site, which controls the competition between the *p-p* and *p-d* couplings. In both the spinel and inverse-spinel structures, there is high concentration of Zn *d*-states close to the VBM. The concentration of In *d*-states in the same region, albeit small, is not negligible. The *d*-states couple strongly to the O *p*-states, therefore.

In the inverse-spinel structure, the Zn ions are distributed over two non-equivalent sites, one of which is the centrosymmetric point. The In atoms are found in only one non-equivalent site. Consequently, the wave-function parity is determined by the states of centrosymmetric Zn atom. The other Zn site weakens the *p-p* coupling at the Γ-point, in other words, reduce the possibilities to form states with odd parity.

In the spinel structure, the In ions occupy only one non-equivalent site, at the centrosymmetric position. Hence, the In states control the parity of the wave function. The concentration of In *d*-states being small in comparison with that of Zn *d*-states, the *p-d* coupling is smaller than in the inverse-spinel structure. Moreover, the single non-equivalent In site strengthens the *p-p* coupling. For this reason, the gap disparity in the spinel structure is small in comparison with the disparity in the inverse-spinel structure.

Walsh *et al.*[18] found no such disparity in the monoclinic IZO structure of In_2ZnO_4, even though the IZO, spinel, and inverse-spinel densities of states are similar. In contrast with the last two structures, however, the IZO structure is asymmetric under inversion. The lower symmetry reduces the number of forbidden dipolar transitions. In other words, the CBM and VBM states have ill-defined parities, the selection rule blocking VBM-to-CBM excitations is washed out, and the optical gap coincides with the fundamental bandgap.

Consider, next, $In_4Sn_3O_{12}$. Table II shows the transition matrix elements from a large number of bands with energies around 0.60 eV below the VBM for the rhombohedral ISO and ISO_i structures. For rhombohedral ISO, O'Neil *et al.*[17] have found that the transition from the VBM to CBM is allowed, a result ratified by our calculations. Our results, nonetheless, disagree with the 0.60 eV gap disparity in Ref. 17. Our computations show that transitions from all bands below the VBM are allowed. Although relatively small, the dipole transition amplitudes for a significant number of bands exceed 10% of the matrix element for the strongest VBM-to-CBM transition. Such transitions contribute significantly to the absorption coefficient. The optical and fundamental bandgaps are, therefore, identical.

The same argument applies to the rhombohedral ISO_i structure, which allows transitions from the VBM to CBM and yields no gap disparity. The initial state of the strongest transition is band 233, 0.44 eV below the VBM, but the magnitude of its transition matrix element is comparable to that of the VBM-to-CBM transition. The symmetry of the rhombohedral ISO_i structure imposes selection rules forbidding transitions from a number of states below the VBM. Nonetheless, the sum of the amplitudes for transitions from states between 0 and 0.67 eV below the VBM for rhombohedral ISO_i and ISO are nearly equal: 19.43 and 19.77 (arbitrary units), respectively. This near coincidence is expected, in view of the *f*-sum rule (i.e., the Thomas–Reiche–Kuhn sum rule) and of the similarity between the two crystal structures.

As discussed in Density of States, in the two model structures for $In_4Sn_3O_{12}$ the combination of In and Sn atoms

TABLE I. Irreducible representations of the conduction-band minimum and occupied Γ-point states near the valence-band maximum for the multi-cation compound In_2ZnO_4 in the spinel and inverse-spinel structures. Only for the undistorted systems is the symmetry identified. In each case the parity of the irreducible representation then dictates the selection rule distinguishing allowed transitions from forbidden ones. In the other cases, the amplitudes of the computed transition matrix elements, shown in arbitrary units, identify the allowed transitions. The energies are measured from the VBM. For each degenerate band, we show occupation and transition amplitudes corresponding to one of the degenerate *i* states.

System	Band	Energy (eV)	Occupation	Symmetry	Transition	Type transition	Amplitude (a. u.)
In_2ZnO_4	63	1.18	0.00	A_{1g}			
Spinel	61, 62	0.00	2.00	E_g	$E_g \rightarrow A_{1g}$	Forbidden	0.00
	58, 59, 60	−0.10	2.00	T_{1g}	$T_{1g} \rightarrow A_{1g}$	Forbidden	0.00
	55, 56, 57	−0.31	2.00	T_{2g}	$T_{2g} \rightarrow A_{1g}$	Forbidden	0.00
	52, 53, 54	−0.44	2.00	T_{1u}	$T_{1u} \rightarrow A_{1g}$	Allowed	36.40
	49, 50, 51	−1.60	2.00	T_{2u}	$T_{2u} \rightarrow A_{1g}$	Forbidden	0.00
In_2ZnO_4	63	0.29	0.00				
Inverse-spinel	62	0.00	2.00			Forbidden	0.00
	60, 61	−0.29	2.00			Forbidden	0.00
	59	−0.36	2.00			Forbidden	0.00
	58	−0.77	2.00			Forbidden	0.00
	57	−0.92	2.00			Forbidden	0.00
	56	−0.93	2.00			Allowed	54.54
	55	−0.99	2.00			Forbidden	0.00

TABLE II. Irreducible representations of the conduction band minimum and occupied Γ-point states near the valence band maximum for the multi-cation compound $In_4Sn_3O_{12}$ in the rhombohedral ISO and ISO_i structures. Only for the undistorted systems is the symmetry identified. In each case the parity of the irreducible representation then dictates the selection rule distinguishing allowed transitions from forbidden ones. In the other cases, the amplitudes of the computed transition matrix elements, shown in arbitrary units, identify the allowed transitions. The energies are measured from the valence band maximum, and the occupation and transition amplitude are shown for a single state listed for each degenerate band.

System	Band	Energy (eV)	Occupation	Symmetry	Transition	Type transition	Amplitude (a. u.)
$In_4Sn_3O_{12}$	250	0.84	0.00				
rhombohedral ISO	249	0.00	2.00			Allowed	2.64
	248	−0.08	2.00			Allowed	2.29
	247	−0.11	2.00			Allowed	1.34
	246	−0.13	2.00			Allowed	1.25
	245	−0.18	2.00			Allowed	0.02
	244	−0.19	2.00			Allowed	0.17
	243	−0.23	2.00			Allowed	0.27
	242	−0.25	2.00			Allowed	0.35
	241	−0.28	2.00			Allowed	0.63
	240	−0.29	2.00			Allowed	0.25
	239	−0.31	2.00			Allowed	0.63
	238	−0.37	2.00			Allowed	1.19
	237	−0.37	2.00			Allowed	1.03
	236	−0.41	2.00			Allowed	0.32
	235	−0.42	2.00			Allowed	0.64
	234	−0.48	2.00			Allowed	0.20
	233	−0.50	2.00			Allowed	1.04
	232	−0.52	2.00			Allowed	0.11
	231	−0.57	2.00			Allowed	0.14
	230	−0.59	2.00			Allowed	2.27
	229	−0.63	2.00			Allowed	1.79
	228	−0.67	2.00			Allowed	1.20
	227	−0.72	2.00			Allowed	0.45
$In_4Sn_3O_{12}$	250	0.89	0.00	A_g			
rhombohedral ISO_i	248, 249	0.00	2.00	E_u	$E_u \to A_g$	Allowed	3.17
	247	−0.07	2.00	A_u	$A_u \to A_g$	Allowed	1.54
	246	−0.09	2.00	A_g	$A_g \to A_g$	Forbidden	0.00
	245	−0.14	2.00	A_g	$A_g \to A_g$	Forbidden	0.00
	243, 244	−0.16	2.00	E_g	$E_g \to A_g$	Forbidden	0.00
	242	−0.20	2.00	A_u	$A_u \to A_g$	Allowed	0.21
	240, 241	−0.22	2.00	E_u	$E_u \to A_g$	Allowed	1.32
	238, 239	−0.25	2.00	E_g	$E_g \to A_g$	Forbidden	0.00
	236, 237	−0.39	2.00	E_u	$E_u \to A_g$	Allowed	0.13
	234, 235	−0.44	2.00	E_g	$E_g \to A_g$	Forbidden	0.00
	233	−0.47	2.00	A_u	$A_u \to A_g$	Allowed	6.94
	232	−0.49	2.00	A_g	$A_g \to A_g$	Forbidden	0.00
	230, 231	−0.52	2.00	E_g	$E_g \to A_g$	Forbidden	0.00
	229	−0.65	2.00	A_g	$A_g \to A_g$	Forbidden	0.00
	227, 228	−0.67	2.00	E_u	$E_u \to A_g$	Allowed	0.75

weakens the *p-d* couplings, a condition that is sufficient to insure congruence between the optical and fundamental bandgaps. The rhombohedral ISO has no inversion symmetry and hence offers another sufficient condition. Therefore, gap disparities are found in neither rhombohedral ISO nor rhombohedral ISO_i. The absorption coefficients in Fig. 3 visually illustrate the conclusions drawn from the transition matrix elements. The vertical dashed lines display the fundamental and optical bandgaps for the studied multi-cation compounds. In panels (a) and (b) (In_2ZnO_4 structures), the vertical lines are separated by the indicated disparities ΔE_g^{OF}. In panels (c) and (d) ($In_4Sn_3O_{12}$ structures), a single vertical line identifies the coincident bandgaps.

Dipolar transitions in the In_2ZnO_4 systems are forbidden for all Γ-point states above the one defining the disparity between optical and fundamental bandgaps, i.e., within the regions between the two vertical dashed lines in Figs. 3(a) and 3(b). Weak absorption – 10^4 times smaller than the absorption coefficients for photon energies above E_g^O – does occur, however, for *k*-points in the vicinity of Γ-point. This behavior, similar to the one found in rutile SnO_2 and bixbyite In_2O_3,[22] indicates that E_g^O is a dark optical bandgap.[22] Under low illumination, the absorption of light for photon energies below the dark gap is insignificant. Under intense irradiation, by contrast, the weak transitions become important and the optical gap shrinks to match the fundamental
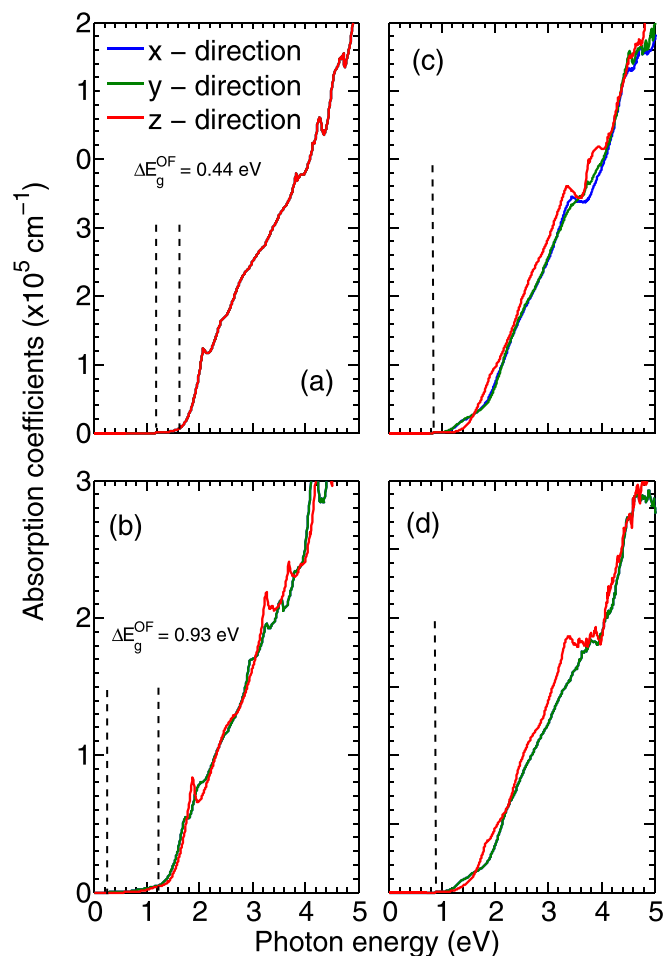
FIG. 3. Absorption coefficients of the multi-cation oxides as functions of the photon energy for different polarization directions. Shown are multi-cation systems based on In_2ZnO_4: (a) spinel, (b) inverse-spinel, and multi-cation systems based on $In_4Sn_3O_{12}$: (c) rhombohedral ISO, and (d) rhombohedral ISO$_i$ structures. In panels (a) and (b) the vertical dashed lines mark the fundamental (left) and optical (right) band gap, while in the panels (c) and (d) a single vertical dashed line indicates the (congruent) fundamental and optical gaps.

gap. There is no disparity between the bright optical and the fundamental gaps.[22]

The rightmost vertical dashed line in each left-hand panel of Fig. 3 marks the dark optical bandgap, the physical parameter of chief importance among the TCO properties. In each right-hand panel, the optical gap coincides with the fundamental bandgap, because both the ISO and ISO$_i$ In$_4$Sn$_3$O$_{12}$ structures violate one or more of the three conditions that, combined, forbid transitions from the VBM to the CBM.[10] As shown by the right-hand panels, for increasing photon frequency ω absorption starts as $\hbar\omega$ exceeds the fundamental band gap. This finding, which contradicts the results of O'Neil *et al.*[17] for the disparity between the optical and the fundamental gaps, shows that the reasoning that explains the optical properties for the binary oxides can be extended to multi-cation compound phases.

Depending on the structure, the absorption can either be isotropic or anisotropic, as Fig. 3 also shows. In systems with well-defined cubic symmetry, such as spinel In$_2$ZnO$_4$, absorption is independent of polarization. For In$_4$Sn$_3$O$_{12}$ in the rhombohedral ISO structure, however, the displacement

of the Sn atoms breaks the symmetry of the structure, and the isotropy of the absorption coefficients. This anisotropy in the rhombohedral In$_4$Sn$_3$O$_{12}$ structure could be associated with the contradiction between our and O'Neil *et al.*'s results. When the measurement of optical absorption is done in a non-single crystal structure, the average of all directions contribute to the observable result. Since the rhombohedral ISO or ISO$_i$ structures have a larger optical bandgap in the direction parallel to the c_0 lattice vector [z-direction in panel (c) and (d) of Fig. 3], in the average with other direction, can "artificially" increase the optical bandgap and mask the real results, leading to an incorrect interpretation of the disparity between the optical and fundamental bandgap.

CONCLUSION

Using DFT, we have computed optical properties for In$_2$ZnO$_4$ and In$_4$Sn$_3$O$_{12}$ multi-cation compounds. We have examined model crystal structures proposed on the basis of experimental and of theoretical results. For In$_4$Sn$_3$O$_{12}$ we have identified a rhombohedral structure (the ISO$_i$ structure), 31.80 meV per formula unit more stable than the rhombohedral ISO structure proposed by O'Neil *et al.*[17] Unlike the asymmetric rhombohedral ISO structure, the ISO$_i$ structure belongs to the $P\bar{3}$ space group, and hence has the point symmetry of the experimental rhombohedral model.

Our study of optical properties is focused on the disparity between the optical and fundamental bandgaps. In particular, we have shown that the concepts proposed in Ref. 10 can be extended from binary oxides to the multi-cation oxides. Thus, the optical bandgap in a multi-cation compound will exceed its fundamental bandgap if the following three conditions are satisfied: (*i*) the crystal structure has inversion symmetry; (*ii*) the conduction-band minimum is formed by cation and O *s*-states; and (*iii*) the *p-d* coupling in the vicinity of the valence-band maximum is strong and the *p-p* coupling, weak.

Examples of systems satisfying the three conditions and hence displaying gap disparities are spinel- and inverse-spinel structured In$_2$ZnO$_4$. In the two structures, the strong *p-d* couplings due to the Zn atoms yield large gap disparities, 0.44 and 0.93 eV, respectively. In contrast, if one or more of the three conditions is violated, the optical and fundamental gaps tend to coincide, as illustrated by the rhombohedral ISO and ISO$_i$ structures for In$_4$Sn$_3$O$_{12}$, and the monoclinic-IZO structure for In$_2$ZnO$_4$.[18]

Wide optical gaps favor transparency, while narrow fundamental gaps benefits the doping process, which in turn raises the conductivity. Control over gap disparities is therefore desirable. Compared with binary compounds, the multi-cation TCOs offer a richer set of alternatives. Our results identified strong *p-d* coupling in the combination $n(In_2O_3)$-$m(ZnO)$. We therefore expect that combination to yield large gap disparities, in contrast with the optical gaps of $n(In_2O_3)$-$m(SnO_2)$ compounds, which we predict to be indistinguishable from their fundamental gaps.

APPENDIX: CRYSTAL STRUCTURE

We have analyzed two configurations for In_2ZnO_4: cubic spinel ($Fd\bar{3}m$, $Z = 2$), and cubic inverse-spinel ($Fd\bar{3}m$, $Z = 2$), all of which are depicted in the middle column of Fig. 4. The cubic-spinel configuration has the formula AB_2O_4, where the site A forms an ideal tetrahedral motif, occupied only by the Zn atoms, while B forms an octahedral motif, occupied by the In atoms. The inverse-spinel (IS) configuration has the same formula, AB_2O_4, but the sites A and B are differently occupied. The (tetrahedral) A site is only occupied by the In atoms, while the (octahedral) B site is randomly occupied by In or Zn atoms, in the 50%–50% proportion. A large unit cell is, therefore, required to properly represent the IS configuration, the treatment of which requires substantial computational effort. We have, therefore, preferred to generate *special quasi-random structures*, which consider the primitive cell of the spinel structure, with the In and Zn atoms especially positioned in the B site, as done previously.[36]

The non-uniform spatial distribution of the In and Zn atoms in the unit cell of inverse-spinel creates a small distortion when the stress tensor is used to optimize the volume and introduces deviations of 0.75% in the computed lattice parameters. We have, therefore, averaged all structural parameters for this structure and present the resulting data in Table III. Compared to the IS configuration, the spinel structure is 0.24 eV per formula unit more stable. The lower energy reflects the tendency of In and Zn atoms to occupy
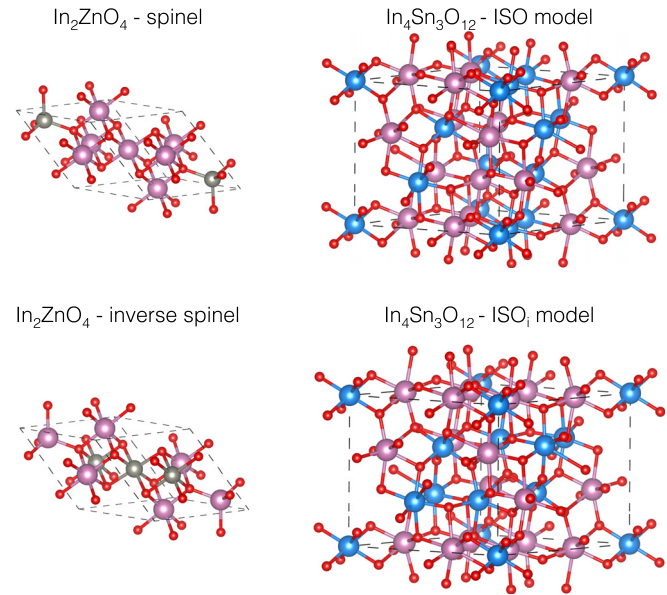

FIG. 4. Crystal structures for the In_2O_3 (bixbyite), In_2ZnO_4 (spinel and inverse-spinel), and $In_4Sn_3O_{12}$ (rhombohedral ISO and rhombohedral ISO_i model). The purple, blue, gray and red balls represent In, Sn, Zn and O, respectively.

high- and low-coordination sites, respectively, as observed, for example, in the unary oxides In_2O_3 bixbyite and ZnO wurtzite.[13,34]

$In_4Sn_3O_{12}$ crystallizes in a rhombohedral ($R\bar{3}$, $a_0 = 6.21$ Å, $\alpha = 99.29°$) structure,[11] which can be represented using a hexagonal cell ($a_0 = 9.46$, $c_0 = 8.86$ Å). This structure comprises two nonequivalent sites with coordination 6 and 7 that we will call $S6$ and $S7$, respectively. The $S6$ sites form an ideal octahedral motif, positioned at the diagonal of the hexagonal representation, and are exclusively occupied by the Sn atoms. The $S7$ sites form a distorted cube with an anion vacancy at one of the vertices,[11] displaced equally on three planes in the hexagonal structure, and are occupied by 1/3 of Sn and 2/3 of In atoms. The experimental results are insufficient to resolve the positions of the Sn and In atoms at the $S7$ sites.[11] On the theoretical front, to find the structure with the globally minimal energy, it suffices to test all possible configurations of In and Sn at the $S7$ sites.

O'Neil *et al.*[17] have proposed a model structure, which we will henceforth call the *rhombohedral ISO model*, for $In_4Sn_3O_{12}$. In the rhombohedral ISO model, depicted by the top right panel in Fig. 4, the Sn atoms are equally displaced on the layers of a hexagonal representation and break the symmetry of the original structure (without cation distinction

TABLE III. Equilibrium lattice parameter, average effective coordination number in number of nearest neighbors (NNN),[35] average weighted bond length for In_2ZnO_4 in spinel and inverse-spinal and $In_4Sn_3O_{12}$ in rhombohedral ISO and rhombohedral ISO_i. The experimental results, when available, are highlighted by bold lettering.[11]

System	Crystal structure	a_0 (Å)	c_0 (Å)	ECN (NNN)	d_{av} (Å)	References
In_2ZnO_4	Spinel	9.05		6.00 (In), 4.00 (Zn)	2.21 (In), 2.06 (Zn)	This work
In_2ZnO_4	Inverse-spinel	9.01		5.00 (In), 6.00 (Zn)	2.15 (In), 2.16 (Zn)	This work
$In_4Sn_3O_{12}$	Rhombohedral	9.65	8.96	6.12 (In), 5.98 (Sn)	2.23 (In), 2.12 (Sn)	DFT[17]
$In_4Sn_3O_{12}$	Rhombohedral	9.64	8.99	6.13 (In), 5.97 (Sn)	2.23 (In), 2.11 (Sn)	This work
$In_4Sn_3O_{12}$	Rhombohedral	**9.46**	**8.86**	**5.99** (In), **5.99** (Sn)	**2.15** (In), **2.12** (Sn)	Exp.[11]

in the $S7$ site). Here, on the basis of our DFT-PBE calculations for $In_4Sn_3O_{12}$, we propose the alternative structure depicted in the bottom-right panel in Fig. 4, which we will refer to as the *rhombohedral ISO$_i$ model*. In the rhombohedral ISO$_i$ model, the point symmetry of the original rhombohedral structure, including inversion, is conserved, as well as coordinations and occupations at the $S6$ and $S7$ sites, and the resulting structure belongs to the $P\overline{3}$ space group. Moreover, there is a different displacement of Sn and In atoms in the structure, which the Sn atoms are closer to each other, a consequence directly of the space group symmetry. Compared to the rhombohedral ISO model,[17] the rhombohedral ISO$_i$ model is 31.80 meV per formula unit more stable.

[1]C. G. Granqvist, Sol. Energy Mater. Sol. Cells **91**, 1529 (2007).

[2]J. J. Berry, D. S. Ginley, and P. E. Burrows, Appl. Phys. Lett. **92**, 193304 (2008).

[3]K. Nomura, H. Ohta, K. Ueda, T. Kamiya, M. Hirano, and H. Hosono, Science **300**, 1269 (2003).

[4]K. Nomura, H. Ohta, A. Takagi, T. Kamiya, M. Hirano, and H. Hosono, Nature **432**, 488 (2004).

[5]H. H. Hsu, C. Y. Chang, and C. H. Cheng, IEEE Electron Device Lett. **34**, 768 (2013).

[6]R. A. Street, T. N. Ng, R. A. Lujan, I. Son, M. Smith, S. Kim, T. Lee, Y. Moon, and S. Cho, ACS Appl. Mater. Interfaces **6**, 4428 (2014).

[7]A. Walsh, J. L. F. Da Silva, and S.-H. Wei, Phys. Rev. B **78**, 075211 (2008).

[8]H. Odaka, Y. Shigesato, T. Murakami, and S. Iwata, Jpn. J. Appl. Phys., Part 1 **40**, 3231 (2001).

[9]A. Walsh, J. L. F. Da Silva, S.-H. Wei, C. Körber, A. Klein, L. F. J. Piper, A. DeMasi, K. E. Smith, G. Panaccione, P. Torelli, D. J. Payne, A. Bourlange, and R. G. Egdell, Phys. Rev. Lett. **100**, 167402 (2008).

[10]F. P. Sabino, R. Besse, L. N. de Oliveira, S.-H. Wei, and J. L. F. Da Silva, Phys. Rev. B **92**, 205308 (2015).

[11]N. Nadaud, N. Lequeux, M. Nanot, J. Jové, and T. Roisnel, J. Solid State Chem. **135**, 140 (1998).

[12]S. Yoshioka, F. Oba, R. Huang, I. Tanaka, T. Mizoguchi, and T. Yamamoto, J. Appl. Phys. **103**, 014309 (2008).

[13]J. L. F. Da Silva, Y. Yan, and S.-H. Wei, Phys. Rev. Lett. **100**, 255501 (2008).

[14]A. S. Gonçalves, M. R. Davalos, N. Masaki, S. Yanagida, A. Morandeira, J. R. Durrant, J. N. Freitas, and A. F. Nogueira, Dalton Trans. **11**, 1487 (2008).

[15]T. Minami, Thin Solid Films **516**, 5822 (2008).

[16]J. L. F. Da Silva, A. Walsh, and S.-H. Wei, Phys. Rev. B **80**, 214118 (2009).

[17]D. H. O'Neil, A. Walsh, R. M. J. Jacobs, V. L. Kuznetsov, R. G. Egdell, and P. P. Edwards, Phys. Rev. B **81**, 085110 (2010).

[18]A. Walsh, J. L. F. Da Silva, Y. Yan, M. M. Al-Jassim, and S.-H. Wei, Phys. Rev. B **79**, 073105 (2009).

[19]W. Sato, S. Komatsuda, Y. Yamada, and Y. Ohkubo, Phys. Rev. B **90**, 235204 (2014).

[20]M. Nagasawa and S. Shionoya, Phys. Lett. **22**, 409 (1966).

[21]A. Schleife, J. B. Varley, F. Fuchs, C. Rödl, F. Bechstedt, P. Rinke, A. Janotti, and C. G. Van de Walle, Phys. Rev. B **83**, 035116 (2011).

[22]F. P. Sabino, L. N. Oliveira, S.-H. Wei, and J. L. F. Da Silva, J. Phys.: Condens. Matter **29**, 085501 (2017).

[23]P. Hohenberg and W. Kohn, Phys. Rev. **136**, B864 (1964).

[24]W. Kohn and L. J. Sham, Phys. Rev. **140**, A1133 (1965).

[25]J. P. Perdew, K. Burke, and M. Ernzerhof, Phys. Rev. Lett. **77**, 3865 (1996).

[26]P. E. Blöchl, Phys. Rev. B **50**, 17953 (1994).

[27]G. Kresse and D. Joubert, Phys. Rev. B **59**, 1758 (1999).

[28]G. Kresse and J. Hafner, Phys. Rev. B **48**, 13115 (1993).

[29]G. Kresse and J. Furthmüller, Phys. Rev. B **54**, 11169 (1996).

[30]J. P. Perdew, Int. J. Quantum Chem. **28**, 497 (1985).

[31]J. Heyd and G. E. Scuseria, J. Chem. Phys. **120**, 7274 (2004).

[32]J. Heyd, G. E. Scuseria, and M. Ernzerhof, J. Chem. Phys. **124**, 219906 (2006).

[33]J. P. Perdew, W. Yang, K. Burke, Z. Yang, E. K. U. Gross, M. Scheffler, G. E. Scuseria, T. M. Henderson, I. Y. Zhang, A. Ruzsinszky, H. Peng, J. Sun, E. Trushin, and A. Görling, Proc. Natl. Acad. Sci. U.S.A. **114**, 2801 (2017).

[34]F. P. Sabino, L. N. de Oliveira, and J. L. F. Da Silva, Phys. Rev. B **90**, 155206 (2014).

[35]J. L. F. Da Silva, J. Appl. Phys. **109**, 023502 (2011).

[36]S.-H. Wei and S. B. Zhang, Phys. Rev. B **63**, 045112 (2001).